Molecular Dynamics Study of Phase Change Mechanisms During Femtosecond Laser Ablation

Xianfan Xu
e-mail: xxu@ecn.purdue.edu

Changrui Cheng

Ihtesham H. Chowdhury

School of Mechanical Engineering,
Purdue University

In this work, Molecular Dynamics (MD) simulation is employed to investigate femtosecond laser ablation of copper, with an emphasis on the understanding of the mechanism of phase change during laser ablation. Laser induced heat transfer, melting, surface evaporation, and material ablation are studied. Theoretically, it has been suggested that under intense femtosecond laser irradiation, the material undergoes a volumetric phase change process; its maximum temperature can be close to or even above the thermodynamic critical point. The MD simulations allow us to determine the transient temperature history of the irradiated material and to reveal the exact phase change process, which explains the mechanisms of femtosecond laser ablation. A finite difference calculation is also performed, which is used to compare results of heating and melting prior to a significant amount of material being ablated. [DOI: 10.1115/1.1797011]

Introduction

In recent years, commercial, turn-key femtosecond pulsed lasers have been rapidly developed and employed in materials processing. Due to the extremely short laser pulse duration, heat diffusion is confined, resulting in more precise machining compared with those obtained with longer laser pulses. On the other hand, femtosecond laser material interaction involves coupled, nonlinear, and non-equilibrium processes, inducing extremely high heating rate (10^{16} K/s) and high temperature gradient (10^{11} K/m) near the laser irradiated surface. The purpose of this work is to use numerical techniques to investigate the rapid phase change process during femtosecond laser ablation. Both finite difference (FD) and molecular dynamics (MD) calculations are carried out.

A large amount of work has been dedicated to the numerical study of laser material interactions. Several finite difference schemes have been reported in the literature. These works implement the two-temperature model first proposed by Anisimov et al. [1], which was later rigorously developed from the Boltzmann transport equation [2]. The two-temperature model considers electrons and the lattice as two sub-systems. The laser energy is first absorbed by electrons and subsequently coupled to the lattice over a time period of several picoseconds. Recently, this model has been extended to compute solid-liquid and liquid-vapor phase change induced by a femtosecond laser pulse [3]. For MD calculations, due to the limitation of computing power, most work has been restricted to systems with a small number of atoms. For example, MD calculations of laser ablation of a dielectric system consisting of 4851 atoms [4] and crystalline silicon containing approximately 23,000 atoms [5] have been reported. A metal system consisting of 160,000 atoms was simulated [6] using the Morse potential function [7]. Heat conduction by the electron gas in metal, which dominated the heat transfer process, could not be predicted by the Morse potential function. Rather, it was simulated using the finite difference method based on the thermal conductivity of electrons in metal. A larger argon crystal of about half a million atoms irradiated by a laser pulse was investigated [8]. Recently, Wang and Xu studied thermal and thermomechanical phenomena during picosecond laser ablation of an argon crystal of a size of two million atoms [9,10]. Generation and propagation of the thermal stress, and the coupling between the temperature field and the stress field were discussed in detail.

In this work, MD simulations are conducted to study femtosecond laser ablation of copper. Over two million atoms are simulated using parallel computing techniques. Laser induced heat transfer, melting, surface evaporation, ablation (i.e., rapid removal of a significant amount of material, also referred to as a volumetric phase change process in this work) are studied. In addition, finite difference (FD) calculations are carried out and results of laser induced heating and melting are compared with those from MD calculations. The emphasis of this work is to investigate the mechanisms of laser ablation. Parameters relevant to laser ablation, such as the transient temperature history and superheating of the melted material are presented.

Theoretical Description of the Mechanisms of Femtosecond Laser Ablation

There are two processes of laser induced material removal: surface evaporation and volumetric liquid-vapor phase transformation [11]. Surface evaporation occurs at any melted surface. During pulse laser heating, however, surface evaporation normally accounts for a small fraction of the total material that is removed, since the high temperature state only lasts for a short period of time. Under high power, short pulse laser irradiation, another material removal mechanism, the volumetric phase transformation termed phase explosion becomes important [12,13]. Phase explosion can be illustrated using the p-v diagram as shown in Fig. 1(*a*). With rapid heating by a laser pulse, it is possible to raise the temperature above the boiling point ''A''. This is because the number of nucleation sites generated within the short heating duration is small. On the other hand, there is a boundary of thermodynamic phase stability, the spinode, which is marked as point ''B'' in Fig. 1(*a*). The spinodal temperature can be calculated from the derivatives of the Gibbs' thermodynamic potential using appropriate equation of state near the critical point. At the spinode, homogeneous (volumetric) nucleation, or phase explosion occurs. The liquid is turned into a mixture of liquid and vapor through an explosion (expansion) process as shown in Fig. 1(*a*) from state B to state C. Therefore, phase explosion is accompanied with melt

Contributed by the Heat Transfer Division for publication in the JOURNAL OF HEAT TRANSFER. Manuscript received by the Heat Transfer Division August 4, 2003; revision received June 3, 2004. Associate Editor: C. P. Grigoropoulos.

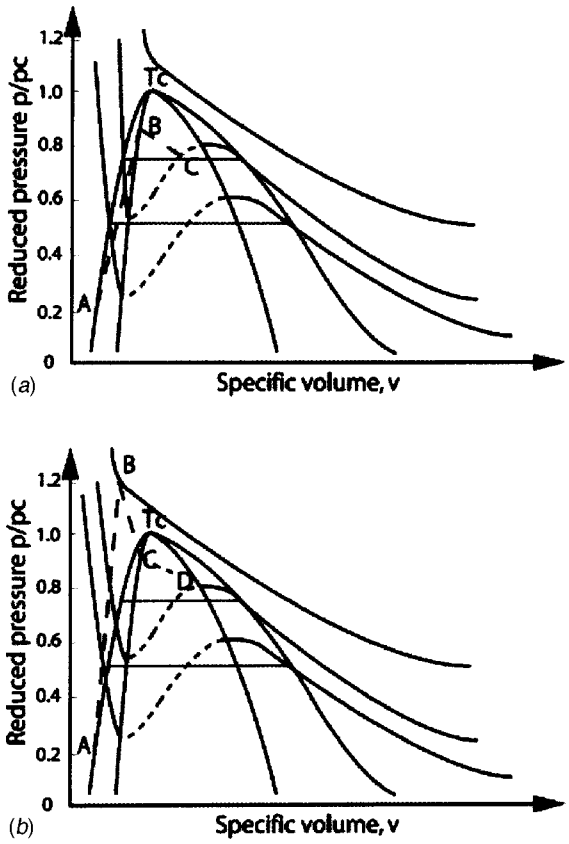

Fig. 1 (*a*) *p-v* diagram of phase explosion at spinode; and (*b*) *p-v* diagram of critical point phase separation

expulsion. Experimental work has shown that phase explosion occurs during nanosecond laser ablation of a metal [11,13].

The physical phenomena occurring in femtosecond laser ablation are much more complicated than those in nanosecond laser ablation. Due to the extremely short heating duration, the time required to transfer energy from the electron system to the lattice is longer than the laser pulse, leading to non-equilibrium between electrons and the lattice. Intense femtosecond laser pulses can cause electron emission. Because the mobility of electrons in dielectrics and semiconductors is low, a localized high ion density results which can exceed the lattice stability limit and cause Coulomb explosion—a type of nonthermal ablation [14,15]. Nonthermal Coulomb explosion is much more significant in dielectrics and semiconductors, while it plays a minor role in metal.

Femtosecond laser also causes an explosive type of material removal. An important factor that needs to be considered here is the time for vapor embryos to grow to nuclei prior to the volumetric phase change taking place. (Embryos smaller than a critical size will collapse, while those larger than the critical radius, called nuclei, will favor growing in order to reduce free energy.) The time for nucleation, or the time lag for phase explosion, has been estimated from the classical nucleation theory to be within 1 and 10 ns [16]. Experimental study showed that this time lag is about 5 ns during nanosecond laser ablation of a nickel target [17]. Since this time lag is longer than 1 ns, nucleation cannot occur during laser heating if the laser pulse is shorter than 1 ns. With the use of a femtosecond laser, heating above the spinodal temperature or even above the critical temperature becomes possible. A phase change process from the super-critical state to a two phase mixture is termed critical point phase separation [18]. The p-v diagram of critical point phase separation is shown in Fig. 1(*b*). Under an extreme heating rate, a material reaches a state above the thermodynamic critical temperature "B", followed by an expansion (relaxation) process during which the nucleation embryos continue to grow. When a sufficient number of nucleation sites are generated in this expansion process, a violent phase change process takes place (state "C" to "D"). The exact point when this phase change occurs (i.e., above or below the critical point) is not known, but is probably dependent on the peak temperature obtained during the process. In the past, such a phenomenon was only discussed in a theoretical context due to lack of means to achieve the required heating rate [18]. However, with femtosecond laser heating, it was suggested that the critical point phase separation could be responsible for ablation [19].

We have conducted many experimental and numerical researches on the phase change process during nanosecond laser ablation [11,13,17]. This work continues our efforts on the investigations of pulsed laser ablation, with the emphasis on the ablation induced by a femtosecond pulse. From the above discussion, information such as the transient temperature during the laser ablation process, the creation of the vapor phase inside the superheated liquid, and the time required to form a two-phase mixture are needed to describe the phase change phenomena induced by a femtosecond laser pulse. The MD calculations conducted in this work are intended to provide detailed descriptions of femtosecond laser ablation.

Numerical Approach

Molecular Dynamics simulation is a computational method to investigate the behavior of materials by computing the molecular or atomic motion governed by a given potential. For copper, a suitable potential is the Morse potential expressed as [7]

$$\Phi(r)=D[e^{-2b(r-r_\varepsilon)}-2e^{-b(r-r_\varepsilon)}] \tag{1}$$

where D is the total dissociation energy and r_ε is the equilibrium distance. The constant b in this equation determines the shape of the potential curve. When $r\rightarrow r_\varepsilon$, the potential $\Phi\rightarrow -D$. At very large separation distance r, $\Phi\rightarrow 0$. Using the potential function, the force between two atoms is obtained as

$$F(r)=-\frac{\partial\Phi(r)}{\partial r}=2Db[e^{-2b(r-r_\varepsilon)}-e^{-b(r-r_\varepsilon)}] \tag{2}$$

The Morse potential has been proven to be a good approximation to the interactions between atoms in fcc metals, and is capable of predicting many material properties [7]. It has been widely used in simulating laser ablation processes [6,20–23]. Although there are other potentials for copper used in literatures, such as the embedded atom method [24], we have chosen the Morse potential since it requires the least amount of computational time and also there is no evidence which potential provides better description for the laser ablation problem. MD simulations of picosecond laser ablation of metal using EAM yielded similar volumetric phase change phenomena as the one obtained in this work [25], although direct comparison is not possible because of the different laser parameters used in the two works (different pulsewidth, fluence, etc.).

The general approach of MD is to obtain atomic positions, velocities, etc. at time $t+\delta t$ based on positions, velocities, and other dynamic information at time t. The equations are solved on a step-by-step basis. Many different algorithms have been developed to solve Eqs. (1) and (2), of which the Verlet algorithm is widely used due to its numerical stability, convenience, and simplicity [26]. In this work, a modified Verlet algorithm is used [9].

In the calculation, most time is spent on calculating forces. However, it is not necessary to calculate forces between all atoms in a computational domain. When two atoms are far enough from each other, the force between them becomes very small (see Eq.

(2)). The distance beyond which the interaction force is negligible is called the cutoff distance (potential cutoff). In this work, r_c is taken as $2.4r_\varepsilon$. At this distance r_c, the potential is about 0.9% of the equilibrium potential D.

Using the two-temperature model, the laser energy is considered absorbed by electrons in copper first, and is then transferred from electrons to the lattice. The governing equation for electrons and the electron-lattice coupling can be obtained from two-temperature model and is expressed as [27]

$$C_e\frac{\partial T_e}{\partial t}=\frac{\partial}{\partial x}\left(k_e\frac{\partial T_e}{\partial x}\right)-G(T_e-T_l)+S \tag{3}$$

The strength of energy coupling between electrons and the lattice is represented by G. The last term S represents absorption of energy by electrons from the laser. The laser source term S is expressed as the standard form for a laser pulse with a Gaussian temporal distribution:

$$S=0.94\frac{1-R}{t_p\delta}J\cdot\exp\left(-\frac{x}{\delta}-2.77\left(\frac{t-t_0}{t_p}\right)^2\right) \tag{4}$$

The use of Eq. (3) for computing energy absorption and diffusion in the electron system is justified. This is because the time for electrons to absorb photon energy and reach thermal equilibrium (electron thermalization time) is short, on the order of 500 fs [28]. This time scale is less than the time for energy to transfer from electrons to the lattice (~ps) and the time of the subsequent phase change process (~10 ps or longer), which is the main focus of this study. In other words, the detailed process of how the electrons reach equilibrium, which occurs much earlier than the lattice structural change, is not important for this work.

The TDMA (Tri-Diagonal Matrix Algorithm) method is used to solve Eq. (3). At each time step, the electron-lattice coupling term $G(T_e-T_l)$ is added to the lattice by scaling the velocities of all atoms in a structural layer by a factor $\sqrt{1+G(T_e-T_l)\,\delta t/E_{k,t}}$, where $E_{k,t}$ is the total kinetic energy in the layer at the time t. This is equivalent to increasing the lattice energy as

$$C_l\frac{\partial T_l}{\partial t}=G(T_e-T_l) \tag{5}$$

Heat conduction in the lattice is always considered in the MD simulation, although it is insignificant compared with the electron conduction in a metal. The change of density due to thermal expansion or phase change is considered by scaling the thermal conductivity and specific heat of electrons in each cell by the ratio of the local density to the original density. Therefore, when expansion happens, the effective thermal conductivity and specific heat decreases, which is consistent with the electron properties of metals [29]. The total energy of the two systems is monitored and compared to the input laser energy at each time step. The procedure of handling heating of the lattice in a MD calculation has been described elsewhere [9].

A significant effect in femtosecond laser heating of metals is the ballistic motion of electrons [30,31]. This effect effectively leads to a greater absorption depth and hence lower surface temperatures [3]. However, no experimental data is available on the ballistic effect in copper, although it is expected to have some effect in all s/p-band metals [31]. As the main emphasis in this work is on identifying the material removal mechanisms rather than comparison with experimental data, inclusion of the ballistic effect is not strictly necessary as it would simply lead to a modification of the optical penetration depth and hence increase the threshold fluences for phase change.

The computational domain consists of 30 fcc (face-centered cubic) unit cells in y and z-directions, and 600 fcc unit cells in the x-direction, which is shown in Fig. 2. The total number of atoms is 2,160,000. The whole computational domain before laser heating is 10.97 nm×10.97 nm×218.65 nm. This computational size is sufficient to track the propagation of the phase change interface in the direction normal to the laser irradiated surface (the x-direction), as well as to maintain a large number of atoms in the y-z cross-sectional area so that macroscopic properties such as temperature can be determined from statistical analysis [9]. Periodic boundary conditions are used in y and z-directions, and free boundary conditions in the x-direction.

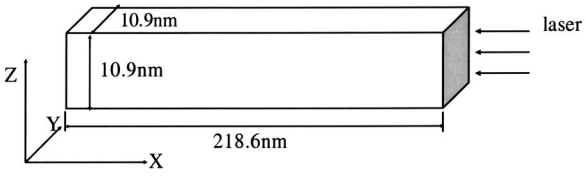

Fig. 2 Schematic of the computational domain

The large number of atoms in the simulation necessitates the use of parallel computing platforms to accelerate computation. At the present time, a cluster of eight PCs is used, each with a 2.0 GHz AMD Athlon processor. The work across the processors is partitioned by dividing the whole domain into eight sub-domains so that the number of atoms for each processor is almost the same. Each processor computes forces and updates positions of all particles in the sub-domain. MPICH, a Message Passing Interface is used, which performs inter-processor communication for atoms close to inter-processor domain boundaries for both computing forces and reassigning atoms based on updated positions. Figure 3 shows the schematic of the domain division and calculation process. For simplicity, a four-node system is illustrated. Interfacial layers are designated in each sub-domain, where the information of the atom positions and velocities is identical in the neighboring sub-domains. During each time step, each subdomain is first calculated by its processor, and atom position and velocity updating and exchanging are carried out on the interfacial layers between sub-domains. In other words, each processor only computes one sub-domain; the interfacial layer does not need to be calculated by both processors as the information is passed from one sub-domain to the other as shown in Fig. 3. Therefore, no extra time is spent on force calculations which are the most time consuming part of the computation. This technique greatly reduces the storage space requirement, and more importantly, the information exchanging load between processors. Calculations show that the overall efficiency of the parallel program is excellent, about 90–92% on eight processors. This implies that the overhead associated with load imbalance and communication is small.

In addition to the MD calculations, finite difference calculations are also carried out. As will be shown later, the FD calculation does not provide correct results about the material removal since it

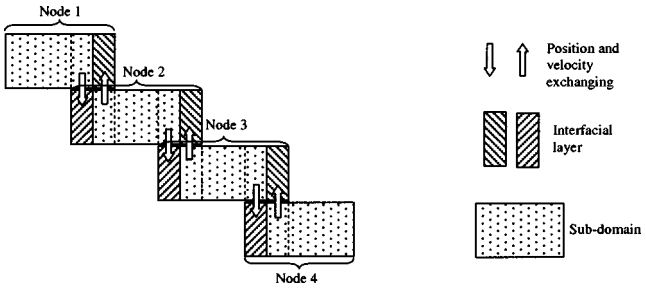

Fig. 3 Schematic of domain division and position and velocity exchange in parallel calculation

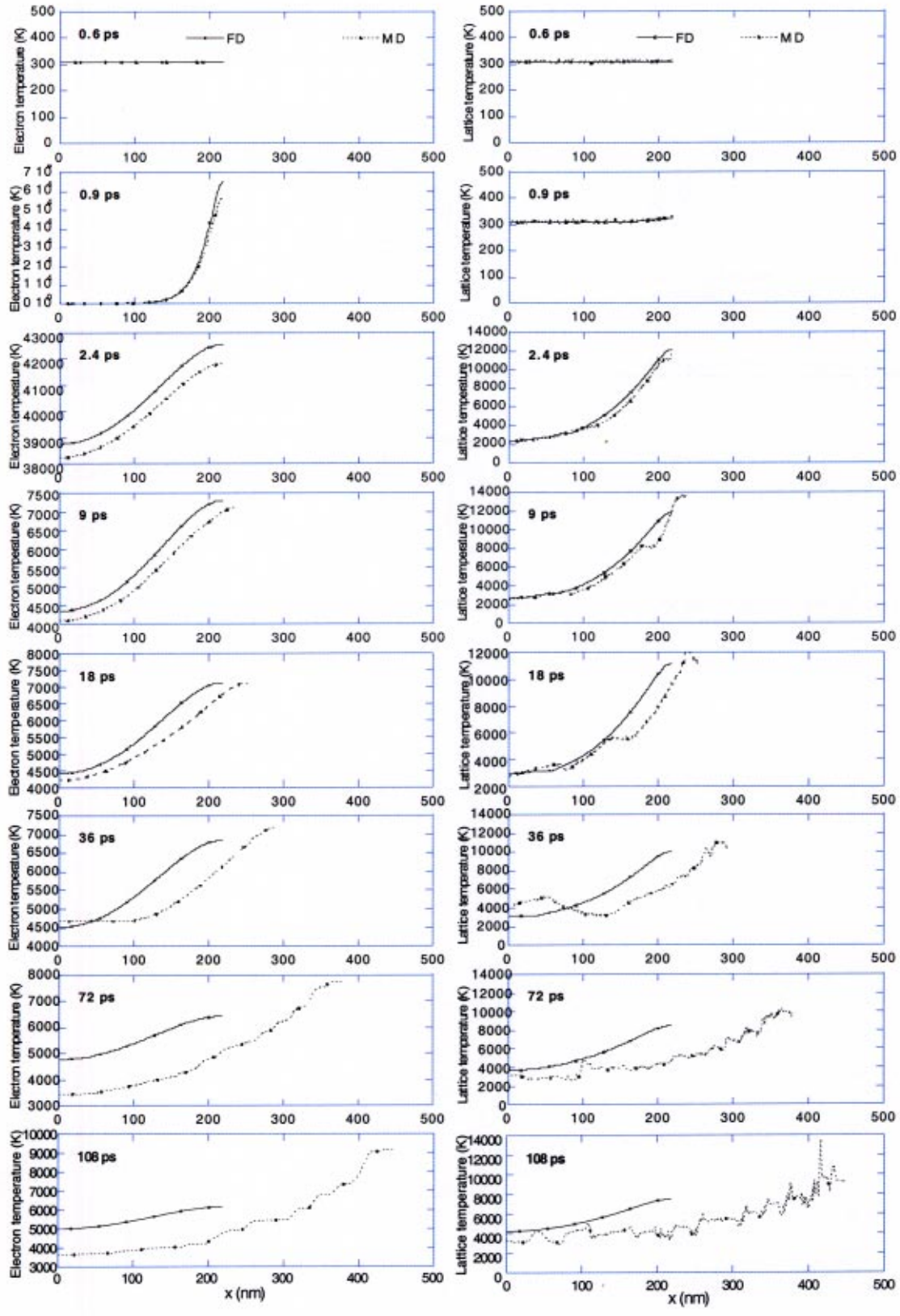

Fig. 4 Comparison of electron (left column) and lattice temperatures (right column) obtained from MD and FD calculations

does not account for the volumetric phase change described previously. The purpose here is to compare with the MD results before the volumetric phase change occurs. The FD calculation is based on the non-equilibrium hyperbolic two-step model [2]. For the present simulation, the model is simplified to consider only one-dimensional heat conduction and the hyperbolic part is neglected to yield a simpler parabolic set of equations. These assumptions are justified as the laser spot size is large compared to

the heat penetration depth and the laser pulse width (100 fs) is long compared to the electron relaxation time [2]. The coupled equations of the model are:

$$C_e\frac{\partial T_e}{\partial t}=\frac{\partial}{\partial x}\left(\kappa_e\frac{\partial T_e}{\partial x}\right)-G(T_e-T_l)+S \tag{6a}$$

$$C_l\frac{\partial T_l}{\partial t}=\frac{\partial}{\partial x}\left(\kappa_l\frac{\partial T_l}{\partial x}\right)+G(T_e-T_l) \tag{6b}$$

It is seen that absorption of laser energy by electrons is modeled in the same way as in the MD calculation, while heat transfer in the lattice is modeled using the heat diffusion equation (Eq. 6(b)). The laser source term S is identical to what is shown in Eq. (4). The initial electron and lattice temperatures are taken to be equal to the room temperature and the top and bottom surfaces of the target are assumed to be insulated.

At high fluences and short pulse widths considered in this study, rapid solid-liquid phase changes are controlled by nucleation dynamics rather than by heat transfer at the phase change interface [32]. At the solid-liquid interface, the relation between the superheating/undercooling at the interface, $\Delta T=T_{sl}-T_m$, and the interface velocity V_{sl} is given by

$$V_{sl}(T_{sl})=V_0\left[1-\exp\left(-\frac{L_{sl}\Delta T}{k_bT_{sl}T_m}\right)\right] \tag{7}$$

where T_{sl} is the temperature of the solid-liquid interface, T_m the equilibrium melting temperature, and L_{sl} the enthalpy of fusion per atom. V_0 is a velocity factor. The energy balance equation at the solid-liquid interface is

$$\kappa_s\left.\frac{\partial T_l}{\partial x}\right|_s-\kappa_{\mathrm{liq}}\left.\frac{\partial T_l}{\partial x}\right|_{\mathrm{liq}}=\rho_s\ V_{sl}\ L_{sl} \tag{8}$$

Procedures of solving Eqs. (5)–(7) have been described elsewhere [3].

In general, material removal by evaporation during femtosecond laser heating can be modeled using the Clausius-Clapeyron equation to provide for superheating at the liquid-vapor interface, the energy loss due to evaporation, and the amount of material evaporated [3,32]. However, it was noticed that evaporation contributes very little to the actual material removal process. It was seen that for femtosecond heating of gold, evaporation would contribute only about 0.1 nm of materials removal [3]. The energy lost due to evaporation is also negligible compared with the energy absorbed by the system. As such, in this calculation, the evaporation process was neglected and the material was allowed to stay liquid past the equilibrium evaporation temperature.

For both calculations, the laser beam is considered uniform in space, with a temporal Gaussian distribution (Eq. (4)) of 100 fs FWHM centered at 1 ps. The laser beam energy is absorbed exponentially in the target, with an absorption depth δ of 12.6 nm. Other parameters used in the calculations are: $C_e=2.1\times10^4$ J/m^3-K, $\kappa_e=386$ W/m-K, $G=4.8\times10^{16}$ W/m^3-K, $C_l=383.817$ J/kg-K, $\kappa_l=0.01\times\kappa_e$, $L_{sl}=2.07\times10^5$ J/kg, $T_m=1358.0$ K, $\rho_s=8.96\times10^3$ kg/m^3, $D=0.3429$ eV, $b=13.588$ nm^{-1}, and $r_e=0.2866$ nm. The laser fluence (absorbed) is 0.4 J/cm^2. Properties used here are considered temperature-independent, since temperature dependent properties near the critical point are not available. However, the uncertainties in the properties will not affect this study since the focus is on the mechanisms of laser ablation, rather than obtaining the absolute thermodynamic parameters at the laser fluence used in the calculation.

Results and Discussion

Figure 4 shows electron and lattice temperature distributions in the target computed using the MD and FD methods. The surface is at the right edge, and laser pulse is incident on the surface from right to left. In the MD simulation, the temperature of the lattice at different locations is calculated as an ensemble average of a domain with a thickness of $2.4r_e$ in the x direction.

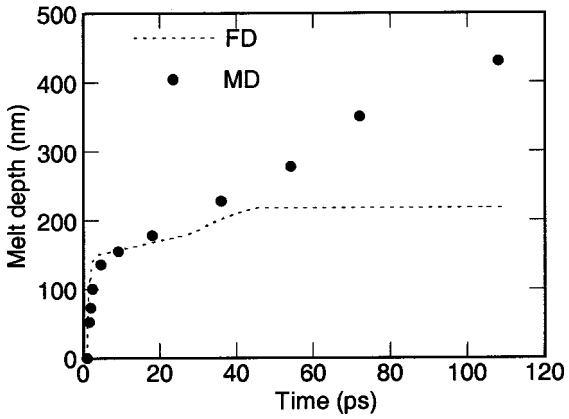

Fig. 5 Comparison of the melt depth obtained from MD and FD calculations

From Fig. 4, it is seen that the electron temperature on the surface increases from room temperature to a very high value (on the order of 10^5 K) within half a picosecond. However, at that time, the lattice temperature only increases tens of degrees. As electrons transfer energy to the lattice, the thermal expansion causes the length of the domain to increase. Note this lattice expansion is computed in the MD simulation only. It is observed from the figures that the results from the two calculations are comparable until about 9 ps. After that time, the results diverge as the FD calculation does not account for thermal expansion and the actual material removal caused by material breakup as observed in the MD calculation. For example, at 18 ps, the length of the MD calculation domain becomes more than 20 nm longer than the length of the FD calculation domain, which does not change with time. Further, at about 30 ps, the material starts break up (as will be seen in Figs. 6 and 7), which leads to a much longer total domain length. This type of volumetric phase change is not accounted for in the FD calculation. The temperature distributions from the FD and MD calculations diverge further after this volumetric phase change occurs.

A plot of the melt front position as a function of time shown in Fig. 5 also indicates that the two calculations yield similar results before liquid-vapor phase change begins. Before 20 ps, the melt depth calculated from MD is slightly larger than that from MD, which is caused by the thermal expansion as seen from the MD results in Fig. 4 and Fig. 6. After about 30 ps, the melt front positions calculated from the two methods start to differ significantly. This is because that the volumetric phase change is not considered in the FD calculation. In Fig. 5, the melt depth from the MD calculation is evaluated as the distance between the solid/liquid interface and the liquid surface, which includes gas bubbles formed inside the liquid (see Figs. 6 and 7) and therefore results in a much longer melt depth. The comparisons of the surface temperature and the melt depth indicate that the two methods provide similar results for heating and solid-liquid phase change prior to the beginning of the volumetric phase change.

The atomic number density at different times computed from the MD simulation is shown in Fig. 6. For solid, the value of number density at the location of a lattice layer is much higher than the average value, and the value at the location between lattice layers is almost zero. For liquid, the atomic number density is uniform due to the lack of periodic structures. For the gas state, the number density is very low compared with the liquid. Therefore, the atomic density shows clearly the state of matter at different locations in the computational domain. Figure 6 indicates that the lattice structure is intact within the first 1 ps or so, which

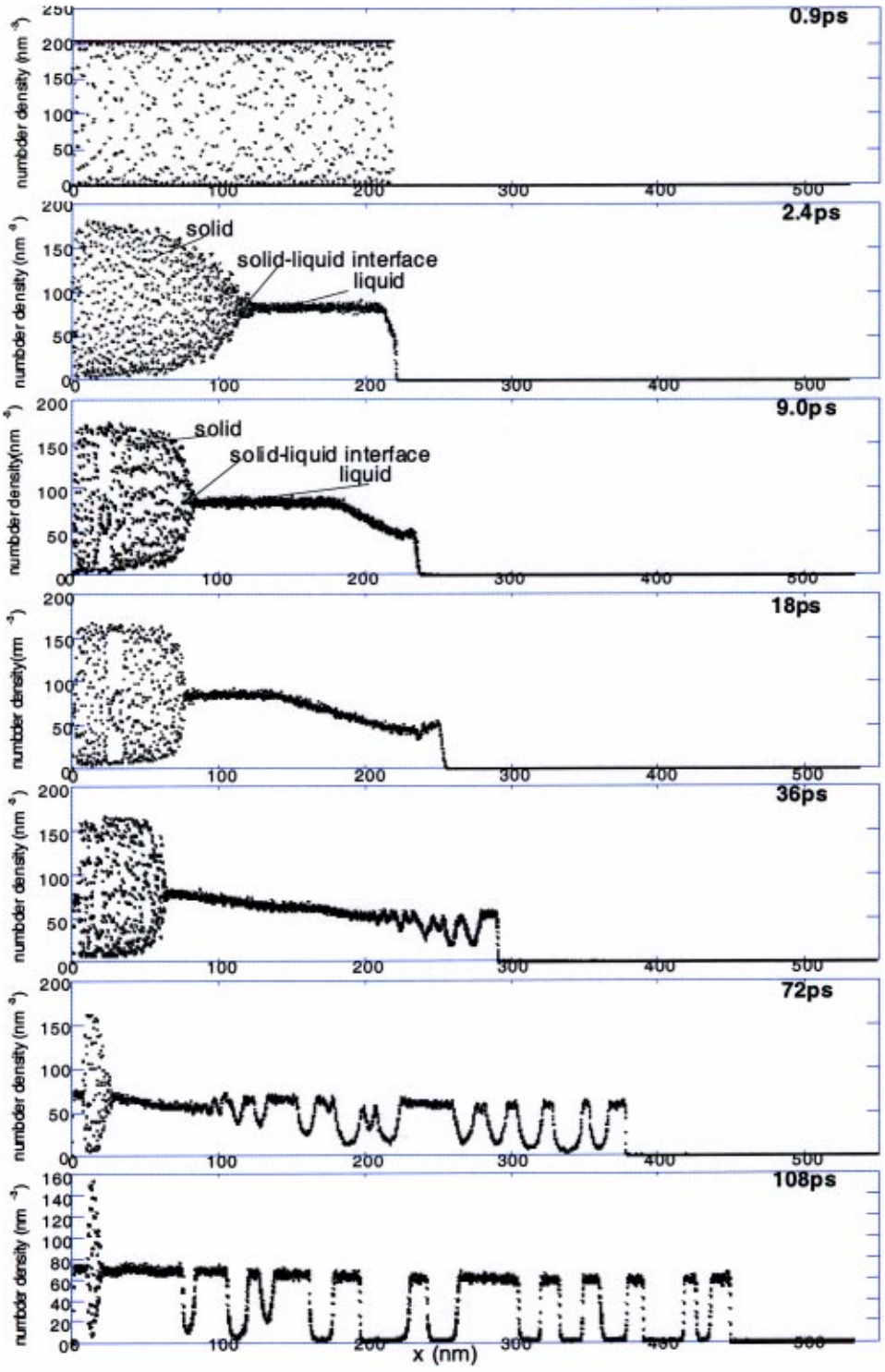

Fig. 6 Atomic number density at different time steps

is reflected by the oscillation of the atomic number density over the entire calculation domain. Melting has occurred at 2.4 ps but most of the target still has the lattice structure. On the surface, the number density drops from a uniform value to almost zero, showing evaporation occurs at the surface. At 9 ps, the melt propagates further into the target, and more atoms are evaporated. Fluctuation of the number density is seen near the surface at 36 ps, indicating bubbles are forming inside the liquid. This will be shown more clearly in Fig. 7. At later times of 72 ps and 108 ps, more bubbles are generated and the sizes of the bubbles grow larger.

Figure 7 presents several snapshots of two-dimensional (z-x) projections of atomic positions. Because of the large number of atoms, the lattice structure, if it exists, cannot be seen clearly in Fig. 7. Rather, this figure provides another way to show the phase change process inside the melted layer. Bubbles are seen at 36 ps. As time progresses, more bubbles grow from inside the domain.

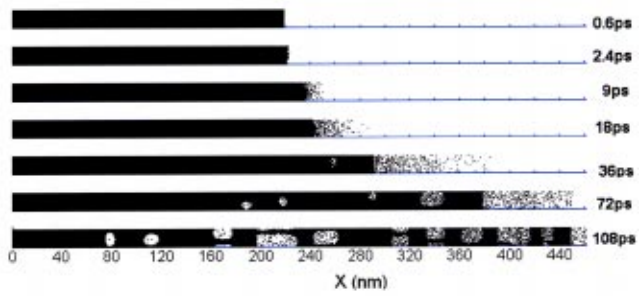

Fig. 7 Atomic positions at different time steps

At 108 ps, the liquid layer is broken into a number of pieces and has essentially ablated. It is found that the velocity of the ablated part near the surface is about 1960 m/s, while the inside part (at the location of 200 nm) is about 900 m/s.

Smaller bubbles may not be seen easily in Fig. 7. In order to observe the exact time when the bubble growth begins, atomic positions are re-plotted over 1/10th of the thickness in the y-direction (about 1 nm) at every time step. Bubbles can be seen as early as 18 ps, which is shown in Fig. 8. These bubbles are not observed in the 18 ps plot in Fig. 7 since they are obstructed by the atoms in front of and behind them along the *y*-direction.

A comparison between Fig. 4 and Fig. 6 provides more information on the relation between phase change and temperature distribution. In Fig. 4, the MD calculations show that there are two lattice temperature plateaus at 9 ps. One is at about 140 nm from the surface (86 nm measured from the bottom, or left). Figure 6 shows that at that time step, the solid-liquid interface is located at 86 nm. The other is at 185 nm, which is the evaporating surface as shown in Fig. 6. It is also seen that the lattice temperatures at these two locations are about 3200 K and 8200 K, respectively. For comparison, the equilibrium melting and boiling points of copper are 1358 K and 2835 K [33]. (The melting temperature of copper computed from the Morse potential is 2090 K [34].) Therefore, strong superheating at these interfaces is observed from the MD calculation.

To better illustrate the temperature history and to explain the ablation process, the transient lattice temperature at the surface is plotted in Fig. 9. It is seen that within a few picosecond, the surface temperature increases rapidly to its peak value of about 1.5×10^4 K. This temperature is above the critical temperature of copper, 7625 K [35]. After that, the temperature decreases due to the expansion of the high temperature material as shown in Figs. 6 and 7. The volumetric phase change does not occur until the expansion process continues for more than 10 ps. Since the volumetric phase change process occurs above the critical point, the critical point phase separation process described previously could have occurred. However, this may not be conclusive since the critical temperature used for comparison is not obtained from the MD calculation. Computations of the critical temperature are currently underway.

Comparing calculation results with experimental data is generally difficult because of the different criteria used in experiments to judge ablation. This is mainly due to the difficulty in distinguishing material removal from surface modification caused by

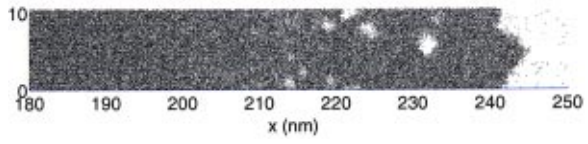

Fig. 8 Atomic position at 18 ps, showing a layer in the *y*-direction from *y*=4 nm to 5 nm

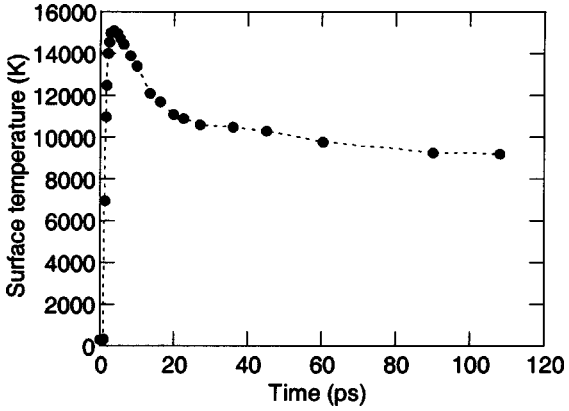

Fig. 9 Surface temperature history

melting and fluid flow. We conducted calculations of 248 nm, 0.5 ps KrF excimer laser ablation of copper, and found that the threshold for volumetric phase change is about 410 mJ/cm^2 (total fluence), while the threshold for melting is about 160 mJ/cm^2. The ablation threshold reported in literature [36] is 170 mJ/cm^2. It is difficult to assess whether the reported threshold value was actually the melting or surface damage threshold, or there was a discrepancy between calculation and experiments. Various factors can contribute to the discrepancy between calculations and experiments, including inaccurate potentials and properties used in the calculation, and oxidation of the surface in a normal experimental condition which leads to a much different absorptivity compared with that used in the calculation.

Conclusions

In summary, femtosecond laser material interaction is studied using numerical simulations. It is found that before the strong, volumetric material removal process takes place, heat transfer and the solid liquid phase change predicted using the FD approach agrees with the result of the MD simulation. At the solid-liquid and liquid-vapor interfaces, strong superheating is observed. The MD simulation predicts a volumetric type of phase change under the evaporating surface, which accounts for material removal during laser machining that is not computed by the FD method.

Acknowledgments

Support to this work by the National Science Foundation and the Office of Naval Research are gratefully acknowledged. The authors also thank Prof. A. Y. Grama of the Department of Computer Science, Purdue University for his help on parallel MD.

Nomenclature

b = constant in Morse potential
C_e = specific heat of electron
C_l = specific heat of lattice
D = total dissociation energy in Morse potential
F = force between two atoms
G = electron-lattice coupling factor
J = laser fluence
k_b = Boltzmann constant
k_e = thermal conductivity of electron
k_l = thermal conductivity of lattice
k_{liq} = thermal conductivity of liquid
k_s = thermal conductivity of solid
L_{sl} = enthalpy of fusion per atom
r = distance between two atoms
R = reflectivity
r_c = cutoff distance
r_ε = the equilibrium distance between two atoms

S = source term of laser heating
t = time
t_0 = center time of the laser pulse
T_e = electron temperature
T_l = lattice temperature
T_m = equilibrium melting temperature
t_p = laser pulse width
T_{sl} = temperature of solid-liquid interface
V_0 = factor to calculate solid-liquid interface velocity
V_{sl} = velocity of solid-liquid interface
x = coordinate in the direction of laser irradiation
Φ = potential between two atoms
δ = absorption depth
ρ_s = density of solid

References

[1] Anisimov, S. I., Kapeliovich, B. L., and Perel'man, T. L., 1974, ''Electron Emission From Metal Surfaces Exposed to Ultra-Short Laser Pulses,'' Sov. Phys. JETP, **39**, pp. 375–377.
[2] Qiu, T. Q., and Tien, C. L., 1993, ''Heat Transfer Mechanisms During Short-Pulse Laser Heating of Metals,'' ASME J. Heat Transfer, **115**, pp. 835–841.
[3] Chowdhury, I. H., and Xu, X., 2003, ''Heat Transfer in Femtosecond Laser Processing of Metal,'' Numer. Heat Transfer, Part A, **44**, pp. 219–232.
[4] Kotake, S., and Kuroki, M., 1993, ''Molecular Dynamics Study of Solid Melting and Vaporization by Laser Irradiation,'' Int. J. Heat Mass Transfer, **36**, pp. 2061–2067.
[5] Herrmann, R. F. W., and Campbell, E. E. B., 1998, ''Ultrashort Pulse Laser Ablation of Silicon: an MD Simulation Study,'' Appl. Phys. A: Solids Surf., **66**, pp. 35–42.
[6] Ohmura, E., Fukumoto, I., and Miyamoto, I., 1999, ''Modified Molecular Dynamics Simulation on Ultrafast Laser Ablation of Metal,'' *Proceedings of the International Congress on Applications of Lasers and Electro-Optics*, Laser Institute of America, Orlando, pp. 219–228.
[7] Girifalco, L. A., and Weizer, V. G., 1959, ''Application of the Morse Potential Function to Cubic Metals,'' Phys. Rev., **114**, pp. 687–690.
[8] Etcheverry, J. I., and Mesaros, M., 1999, ''Molecular Dynamics Simulation of the Production of Acoustic Waves by Pulsed Laser Irradiation,'' Phys. Rev. B, **60**, pp. 9430–9434.
[9] Wang, X., and Xu, X., 2002, ''Molecular Dynamics Simulation of Heat Transfer and Phase Change During Laser Materials Interaction,'' ASME J. Heat Transfer, **124**, pp. 265–274.
[10] Wang, X., and Xu, X., 2002, ''Molecular Dynamics Simulation of Thermal and Thermomechanical Phenomena in Picosecond Laser Material Interaction,'' Int. J. Heat Mass Transfer, **46**, pp. 45–53.
[11] Xu, X., 2001, ''Heat Transfer and Phase Change in Pulsed Excimer Laser Ablation of Metal,'' Annual Review of Heat Transfer, **12**, C.-L. Tien, V. Prasad, and F. P. Incropera, eds., Bell House, New York, pp. 79–115.
[12] Kelly, R., and Miotello, A., 1996, ''Comments on Explosive Mechanisms of Laser Sputtering,'' Appl. Surf. Sci., **96–98**, pp. 205–215.
[13] Song, K. H., and Xu, X., 1998, ''Explosive Phase Transformation in Pulsed Laser Ablation,'' Appl. Surf. Sci., **127**, pp. 111–116.
[14] Siders, C. W., Cavalier, A., Sokolowski-Tinten, K., Toth., Cs., Guo, T., Kammler, M., Horn von Hoegen, M., Wilson, K. R., von der Linde, D., and Barty, C. P. J., 1999, ''Detection of Nonthermal Melting by Ultrafast X-Ray Diffraction,'' Science, **286**, pp. 1340–1342.
[15] Henyk, M., Wolfframm, D., and Reif, J., 2000, ''Ultra Short Laser Pulse Induced Charged Particle Emission From Wide Bandgap Crystals,'' Appl. Surf. Sci., **168**, pp. 263–266.
[16] Skripov, V. P., 1974, *Metastable Liquids*, John Wiley & Sons, New York.
[17] Xu, X., and Willis, D. A., 2002, ''Non-Equilibrium Phase Change in Metal Induced by Nanosecond Pulsed Laser Irradiation,'' ASME J. Heat Transfer, **124**, pp. 293–298.
[18] Skripov, V. P., and Skripov, A. V., 1979, ''Spinodal Decomposition (Phase Transition via Unstable States),'' Soviet Physics Uspekhi, **22**, pp. 389–410.
[19] Vidal, F., Johnston, T. W., Laville, S., Barthelemy, O., Chaker, M., Le Drogoff, B., Margot, J., and Sabsabi, M., 2001, ''Critical-Point Phase Separation in Laser Ablation of Conductors,'' Phys. Rev. Lett., **86**, pp. 2573–2576.
[20] Constantoudis, V., and Nicolaides, C. A., 2001, ''Nonhyperbolic Escape and Changes in Phase-Space Stability Structures in Laser-Induced Multiphoton Dissociation of a Diatomic Molecule,'' Phys. Rev. E, **64**, p. 056211.
[21] Ohmura, E., Fukumoto, I., and Miyamoto, I., 2000, ''Molecular Dynamics Simulation of Ablation Process With Ultra-Short Pulsed Laser,'' Proc. SPIE, **4088**, pp. 84–89.
[22] Nedialkov, N. N., Imamova, S. E., and Atanasov, P. A., 2004, ''Ablation of Metals by Ultrashort Laser Pulses,'' J. Phys. D, **37**, pp. 638–643.
[23] Atanasov, P. A., Nedialkov, N. N., Imamova, S. E., Ruf, A., Hügel, H., Dausinger, F., and Berger, P., 2002, ''Laser ablation of Ni by Ultrashort Pulses: Molecular Dynamics Simulation,'' Appl. Surf. Sci., **186**, pp. 369–373.
[24] Foiles, S. M., Baskes, M. I., and Daw, M. S., 1986, ''Embedded-Atom-Method Functions for the fcc Metals Cu, Ag, Au, Ni, Pd, Pt, and Their Alloys,'' Phys. Rev. B, **33**, pp. 7983–7991.
[25] Schäfer, C., Urbassek, M., and Zhigilei, L. V., 2002, ''Metal Ablation by Picosecond Laser Pulses: A Hybrid Simulation,'' Phys. Rev. B, **66**, pp. 115404-1–115404-8.
[26] Allen, M. P., and Tildesley, D. J., 1987, *Computer Simulation of Liquids*, Clarendon Press, Oxford.
[27] Häkkinen, H., and Landman, U., 1993, ''Superheating, Melting and Annealing of Copper Surfaces,'' Phys. Rev. Lett., **71**, pp. 1023–1027.
[28] Sun, C.-K., Vallée, F., Acioli, L. H., Ippen, E. P., and Fujimoto, J. G., 1994, ''Femtosecond-Tunable Measurement of Electron Thermalization in Gold,'' Phys. Rev. B, **50**, pp. 15337–15347.
[29] Berman, R., 1976, *Thermal Conduction in Solids*, Clarendon Press, Oxford.
[30] Brorson, S. D., Fujimoto, J. G., and Ippen, E. P., 1987, ''Femtosecond Electronic Heat-Transport Dynamics in Thin Gold Films,'' Phys. Rev. Lett., **59**, pp. 1962–1965.
[31] Hohlfeld, J., Wellershoff, S.-S., Güdde, J., Conrad, U., Jähnke, V., and Matthias, E., 2000, ''Electron and Lattice Dynamics Following Optical Excitation of Metals,'' Chem. Phys., **251**, pp. 237–258.
[32] Xu, X., Chen, G., and Song, K. H., 1999, ''Experimental and Numerical Investigation of Heat Transfer and Phase Change Phenomena During Excimer Laser Interaction With Nickel,'' Int. J. Heat Mass Transfer, **42**, pp. 1371–1382.
[33] Lide, D. R., 2001, *CRC Handbook of Chemistry and Physics*, CRC Press, Boca Raton.
[34] Wang, X., 2004, ''Thermal and Thermomechanical Phenomena in Picosecond Laser Copper Interaction,'' ASME J. Heat Transfer, **126**, pp. 355–364.
[35] Young, D. A., and Alder, B. J., 1971, ''Critical Point of Metals From the van der Waals Model,'' Phys. Rev. E, **3**, pp. 364–371.
[36] Preuss, S., Demchuk, A., and Stuke, M., 1995, ''Sub-Picosecond UV Laser Ablation of Metals,'' Appl. Phys. A: Solids Surf., **61**, pp. 33–37.